On the Unsteady Steepening of Short Gravity Waves Near the Crests of Longer Waves in the Absence of Generation or Dissipation

Charles Peureux, Fabrice Ardhuin, Pedro Veras Guimarães

JGR Oceans

RESEARCH ARTICLE
10.1029/2020JC016735

Special Section:
Remote Sensing of Ocean Surface Currents Using Doppler Techniques From Planes and Satellites

On the Unsteady Steepening of Short Gravity Waves Near the Crests of Longer Waves in the Absence of Generation or Dissipation

Charles Peureux[1], Fabrice Ardhuin[1], and Pedro Veras Guimarães[2,3]

[1]Laboratoire d'Océanographie Physique et Spatiale, University Brest, CNRS, Ifremer, IRD, Brest, France, [2]LHEEA Lab UMR6598, École Centrale de Nantes, Nantes, France, [3]Now at France Energies Marines, Bretagne, France

Abstract The wave action equation provides a general framework that has been applied to the conservative hydrodynamic interactions between short and long surface waves. So far, only a limited range of solutions have been investigated. Here, we show that the wave action equation predicts that groups of short waves propagating over long monochromatic waves are unstable. We demonstrate theoretically and numerically, a new ratchet-type instability that progressively condenses short wave action around the long wave crests due to the correlation of phase speed and action fluctuations. This instability is of particular interest because it may lead to a higher probability of breaking for short waves propagating in directions within ±35 degrees of the dominant waves direction. This preferred breaking could has a strong impact on cross- and down-wind slope statistics and thus air-sea exchanges and remote sensing.

Plain Language Summary Short waves riding on long waves tend to focus their energy near the crest of the long waves. This focusing is most pronounced for short waves propagating within 35 degrees of the long wave direction, and may lead to a preferential breaking of short waves. This effect may explain the relatively low energy observed in short waves that propagate near the direction of the long waves.

Key Points:

- Wave trains linearly modulated by longer waves are unstable
- This instability leads to a progressive steepening on the crest of the longer waves

Correspondence to:
F. Ardhuin,
ardhuin@ifremer.fr

Citation:
Peureux, C., Ardhuin, F., & Guimarães, P. V. (2021). On the unsteady steepening of short gravity waves near the crests of longer waves in the absence of generation or dissipation. *Journal of Geophysical Research: Oceans*, *126*, e2020JC016735. https://doi.org/10.1029/2020JC016735

Received 22 AUG 2020
Accepted 23 NOV 2020

1. Introduction

The evolution of random wave fields is a complex problem that has often been treated as a spatially homogeneous or stationary process in which nonlinear wave evolution is represented by 4-wave nonlinear interactions that control the cascade of energy to shorter components with a source of energy from the wind and dissipation by wave breaking (e.g., Hasselmann, 1962; Phillips, 1985). A particular difficulty of the problem is the interaction of multiple scales that introduce effective non-homogeneities, in particular the short waves are expected to respond to the orbital velocities and apparent gravity of the long waves. Recent parameterizations of the spectral wave dissipation have used empirical representations of enhanced breaking of short waves induced by long waves (Donelan et al., 2012; Romero, 2019). This enhanced breaking may explain a large change in the energy level of waves with periods 1–2 s. However, it requires a detailed justification. Here, we will ignore the effect of the short wave nonlinearity that are discussed by Zhang and Melville (1981), and that are certainly important for the eventual evolution of short waves toward breaking. Instead we focus on the nonhomogeneity of linear shorter wave components that is caused by the presence of linear longer wind-generated waves. This effect is generally called modulation. Very similar effects occur when surface gravity waves interact with internal waves (Lewis et al., 1974) or much longer gravity waves such as tides (Ardhuin et al., 2012).

Much of the previous modulation theory and observation work was motivated by the analysis of remote sensing data, in particular the modulated power of microwave radar signals backscattered from short gravity-capillary waves, which is routinely used to measure wind and waves. These investigations have produced very useful theoretical and empirical transfer functions in which the local wind speed and direction play an important role (e.g., Hara et al., 2003; Hasselmann et al., 1985; Keller & Wright, 1975). The early works were also associated to possible net growth or decay of long waves as an indirect interaction of long waves and wind through the presence of short waves (Garrett & Smith, 1976; Hasselmann, 1971; Longuet-Higgins, 1969). Such effects may indeed be relevant to swell dissipation or the generation of the long-period fore-runners described by Munk et al. (1963).

Our purpose differs from these previous works as we focus on not-so-short modulated components, with typical wavelengths around 1 m. For these wavelengths, and for the average wind speed of 7 m/s, a typical growth rate given by Equation 1 in Plant (1982) is $\beta \approx 0.01$ s^{-1}. Over a typical long wave period of 10 s, this gives a growth of only 10%, which we shall neglect. Our interest is the intermittent variability of wave properties, including the mean energy level of the not-so-short waves as a function of direction. One particular motivation for this study is that the energy balance of waves beyond two times the dominant frequency requires some poorly understood "cumulative dissipation" (e.g., Ardhuin et al., 2010; Banner & Morison, 2010; Banner et al., 2002), which may be related to modulation-type processes, possibly associated with steep long waves (Kharif, 1990). Recent observations of meter-scale waves have revealed a suppressed energy level for short waves aligned with the dominant waves (Leckler et al., 2015; Peureux et al., 2018), that cannot be explained by nonlinear 4-wave interactions alone (Peureux, 2017).

It has been recognized for a long time that the dominant waves may organize the evolution of the shorter components by many modulation processes (Longuet-Higgins & Stewart, 1960, hereinafter LH&S), with a possible influence on the spectra of both short and long waves (Banner et al., 1989; Hasselmann, 1971). We have thus decided to revisit the modulation effect for meter-scale short gravity waves in the presence of longer waves. Here, we consider a highly simplified model without sources or sinks of energy, following the classic paper of LH&S. This conservative model is known to be unrealistic in the case of waves over tidal currents, for which wave breaking severely limits the predicted steepness (Ardhuin et al., 2012). Still it exhibits some interesting behavior that has not been described before. In particular, we find that the short wave steepness can be much larger than predicted by LH&S.

The theoretical model is described in Section 2. Section 3 presents the solutions and describes the importance of the terms neglected by LH&S. Section 4 gives a prediction for an envelope instability that is verified numerically. These results are then discussed in Section 5 in the context of random wave breaking and a cumulative effect of long waves on short waves.

2. Problem Statement

Here, we consider a narrow-band field of short waves propagating over a varying large scale velocity field with a horizontal component $\boldsymbol{U}$ and a vertical component W in deep water. The short waves are characterized by an energy density E per unit horizontal surface, a wave vector $\boldsymbol{k}$, an intrinsic radian frequency $\sigma = \sigma(k)$, and an associated action density (e.g., Phillips, 1977)

$$N = \frac{E}{\sigma}. \tag{1}$$

The short waves have intrinsic phase velocity $C = \sigma / k$ and group velocity $C_g = \partial\sigma / \partial k$. The distribution of the short wave energy in space and time is given by the wave-action conservation equation and the conservation of crests (Bretherton & Garrett, 1968; Phillips, 1977),

$$\partial_t N + \nabla \cdot \left[\left(\boldsymbol{C}_g + \boldsymbol{U} \right) N \right] = 0 \tag{2}$$

$$\partial_t \boldsymbol{k} + \nabla \left(\sigma + \boldsymbol{k} \cdot \boldsymbol{U} \right) = 0, \tag{3}$$

where $\nabla = \left[\partial_x, \partial_y \right]$, provided the external current varies slowly compared to the short waves wave length, and neglecting other sources and sinks of energy such as wind input or breaking dissipation. The short wave energy is related to the local envelope amplitude a as given by Equation 4.11 in LH&S,

$$E = \frac{1}{2} \rho g a^2 \left(1 + \frac{1}{2g} \partial_t W \right). \tag{4}$$

Here, we assume that the short waves are in deep water, so that the radian frequency σ and wave number k are related by the dispersion relation

$$\sigma^2 = g'k, \tag{5}$$

where the apparent gravity g' is the gravity acceleration modified by the long wave induced downward vertical acceleration

$$g' = g\left(1 + \frac{1}{g}\partial_t W\right). \tag{6}$$

which slightly differs from the factor in Equation 4. This was not taken into account in LH&S but it is taken into account in later works (e.g., Elfouhaily et al., 2001; Longuet-Higgins, 1991). In deep water, the group speed is related to the phase velocity through

$$C_g = \frac{C}{2} = \frac{1}{2}\sqrt{\frac{g'}{k}}. \tag{7}$$

Together with Equations 5–7, the system of Equations 2 and 3 governs the evolution of the short waves envelope.

We consider a large-scale flow U given by a deep-water monochromatic longer wave of steepness $\varepsilon_L \ll 1$, wave number k_L, radian frequency σ_L, phase speed $C_L = \sigma_L / k_L$, and a phase $\psi = k_L x - \sigma_L t$

$$U = \varepsilon_L C_L \cos\psi, \tag{8}$$

the vertical velocity

$$W = \varepsilon_L C_L \sin\psi \tag{9}$$

and the apparent gravity

$$g' = g\left(1 + \varepsilon_L M_g \cos\psi\right), \tag{10}$$

where $M_g = -1$ (Phillips, 1977). The long wave orbital velocity given by Equation 8 is associated with a long wave surface elevation $\varepsilon_L / k_L \cos\psi$, so that $\psi = 0^\circ$ corresponds to the crests and $\psi = 180^\circ$ to the troughs.

LH&S proposed solutions for the 1D case in which they neglected the gradients of the short waves group velocity compared to the gradients of the orbital currents. It simplified greatly the algebra and lead them to a general first order solution for any short waves modulated variable

$$X(\psi) = X_i\left(1 + \varepsilon_L M_X \cos\psi\right), \tag{11}$$

where the property X of the short waves only depends on the long wave phase and X_i is the mean value of X. M_X is usually called the modulation transfer function (MTF) for the variable X. M_X is of the order of unity for most variables, especially $M_N = 1$ and $M_k = 1$ in the LH&S approximate solution.

In the following, we investigate the modulation in more general conditions, and this departure from the mean short waves behavior, normalized by the long wave steepness, is a periodic function of time and space,

$$\Delta X(x,t) = \frac{X(x,t) - X_i}{\varepsilon_L X_i}, \tag{12}$$

and the MTF M_X in Equation 11 appears in the Fourier series expansion of ΔX as a ψ-periodic function:

$$\Delta X(x,t) = M_X \cos(\psi + \varphi_X) + \sum_{n=2}^{\infty} M_{X,n} \cos\left[n\psi + \varphi_{X,n}\right] \tag{13}$$

This generalization of the modulation is particularly necessary when the modulation is not stationary. From now on, we will often refer to the maximum modulation after a given time to characterize the short waves field.

For simplicity, we consider the problem in which all quantities are invariant along the y-axis, that is, along the long wave crests, so that k_y remains constant along the propagation, and all y partial derivatives are cancelled. This assumption transforms Equations 2 and 3 to their simplified versions

$$\partial_t N + \partial_x\left[\left(\gamma C / 2 + U\right)N\right] = 0 \tag{14}$$

$$\partial_t k_x + \partial_x\left[\left(C / \gamma + U\right)k_x\right] = 0, \tag{15}$$

where $\gamma = k_x / k$ is the cosine of the short waves propagation direction, which will be used for numerical simulations. Changing variables from N and k_x to N and C, with $C = \sqrt{g' / k}$, gives the alternative set of equations, which will be used for analytical calculations,

$$\begin{aligned}&\left[\partial_t + \left(\frac{\gamma}{2}C + U\right)\partial_x\right]N = \\ &-N\left(3\gamma^2 - 2\right) / \left(2\gamma\right)\partial_x C - N\left(1 - \gamma^2\right)C / \left(2\gamma g'\right)\partial_x g' - N\partial_x U\end{aligned} \tag{16}$$

$$\begin{aligned}&\left[\partial_t + \left(\frac{\gamma}{2}C + U\right)\partial_x\right]C = \\ &\left(\gamma^2 C / 2\right)\partial_x U + C / \left(2g'\right)\left[\partial_t + \left(\gamma C + U\right)\partial_x\right]g',\end{aligned} \tag{17}$$

with derivation details given in Appendix A.

At time $t = 0$, a monochromatic and unidirectional short wave is considered, with a slight deviation along the long wave direction that can encompass any kind of random modulation by the latter, considering the modulation of the order of the long wave steepness, in other words

$$N\left(t = 0, x\right) = N_i + \varepsilon_L \delta N\left(x\right) \tag{18}$$

$$C\left(t = 0, x\right) = C_i + \varepsilon_L \delta C\left(x\right) \tag{19}$$

$$k_x\left(t = 0, x\right) = \gamma_i k_i + \varepsilon_L \delta k_x\left(x\right) \tag{20}$$

with

$$\delta C\left(x\right) = \frac{1}{2}\left[M_g \cos\psi - \gamma_i \frac{\delta k_x\left(x\right)}{k_i}\right] + \mathcal{O}\left(\varepsilon_L^2\right). \tag{21}$$

We may also consider more general initial conditions,

$$\delta N\left(t = 0\right) / N_i = M_{N,i} \cos\psi + \sum_{n=2}^{\infty}\left(M_N\right)_{n,i} \cos n\psi \tag{22}$$

$$\delta k_x\left(t = 0\right) = \gamma_i k_i\left[M_{k,i} \cos\psi + \sum_{n=2}^{\infty}\left(M_k\right)_{n,i} \cos n\psi\right]. \tag{23}$$

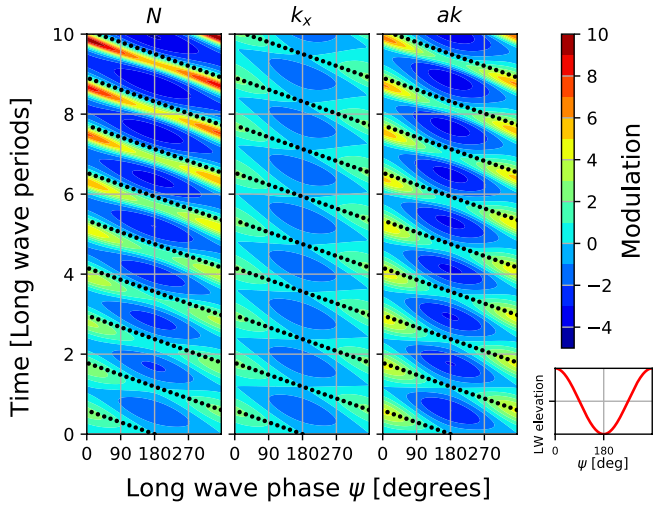

Figure 1. Evolution of short wave properties, action N, wavenumber k and slope ak, in the frame of reference moving with the long wave phase ψ, with $\psi = 0$ corresponding to the long wave crest. The short wave quantities are normalized by the long wave slope ε_L, following the definition of the modulation in Equation 12. The case shown here is for $k_i/k_L = 10$, $\varepsilon_L = 0.1$, $\gamma_i = 1$ and Co = 0.1, starting with a uniform distribution of N and k at $t = 0$. The black dots correspond to successive positions of a linear wave group starting from the trough of the long wave profile and propagating at apparent speed of the short wave groups $0.5C_i$ (see Appendix C).

LH&S initial condition corresponds to $M_{N,i} = M_{k,i} = 1$ and $(M_N)n,i = (M_k)n,i = 0, n \geq 2$. In the following, initial conditions harmonics with $n \geq 2$ will be set to zero for simplicity: we have found that these give perturbations that do not qualitatively change the nature of the solutions.

As a result the initial condition on C is (see Appendix A for more details),

$$C\left(t = 0\right) = C_i\left(1 + \varepsilon_L M_{C,i} \cos\psi\right) \tag{24}$$

at order ε_L, where $M_{C,i} = 0.5\left(M_g - \gamma_i^2 M_{k,i}\right)$.

To summarize, our problem is fully determined by the initial conditions for the short wave wavenumber and action $M_{k,i}(t = 0, x)$ and $M_{N,i}(t = 0, x)$ and 3 parameters, namely the long wave steepness ε_L, the initial scale ratio k_i/k_L, and the short waves propagation direction with respect to the long wave θ_i, or $\gamma_i = \cos\theta_i$. Simulation results are linear in N_i, and independent of the short waves initial steepness.

In the following, the coupled Equations 14 and 15, together with initial conditions 22 and 23 are solved numerically using a procedure detailed in Appendix B and summarized here. As spatially periodic solutions are sought, the simulation spatial domain is reduced to a single long wave length, from $\psi = 0^\circ$ to $\psi = 360^\circ$, with periodic boundary conditions. The problem is solved in a frame moving with the long wave phase velocity. Following up on our interest in short wave breaking, we will particularly focus on the long wave crests, $\psi = 0^\circ$, because the largest short wave steepness is obtained there.

3. Modulation of Two Collinear Wave Trains

3.1. Numerical Simulation

We first consider the simplified 1D configuration where short and long waves are aligned along the x-axis. The short waves do not refract and $\gamma = \gamma_i = 1$ is a constant for the moment. Starting from a uniform distribution, the evolution of short wave action N, wavenumber k_x and short waves steepness ak is shown in Figure 1 for $k_i/k_L = 10$ and $\varepsilon_L = 0.1$.

The space and time evolution of the wavenumber k_x is nearly periodic, with higher values (shorter wavelengths) around the crests of the long waves. Away from the long wave crests, there is a local maximum that travels at the speed of a short wave group with a position shown with the dotted line. The pattern of the action and steepness are similar except that they are clearly not periodic: the wave packet that starts from the trough gains action and steepness each time it goes over a long wave crest, but it only loses part of that gain as it goes in the following trough. Conversely, a wave packet that starts from the wave crest loses action and steepness as it goes over a trough, but only recovers some of that when going over the next crest. What happens is a progressive condensation of action along the trajectory of the first short wave group, the one starting from the trough, and the passage of the wave crests. As the total action is conserved, this gain of one wave group goes with a loss of the neighboring wave groups.

Because the long wave orbital contribution converges on the forward face of the long waves, the increase in short wave action occurs one-quarter of period later, that is, on the crest. This effect is already present in the LH&S solution. What we find here, is that the additional change in advection velocity due to the modulation of the short wave group speed gives an additional amplification. This amplification has a nonzero mean effect because the modulations of N and $C_g = 0.5\sqrt{g/k}$ are correlated: the average perturbation in the advection of action is a product $C_g'N'$ that on average is not zero because of the phase relation between N and k. As a result, every long wave cycle brings a little more convergence and the maximum value of N

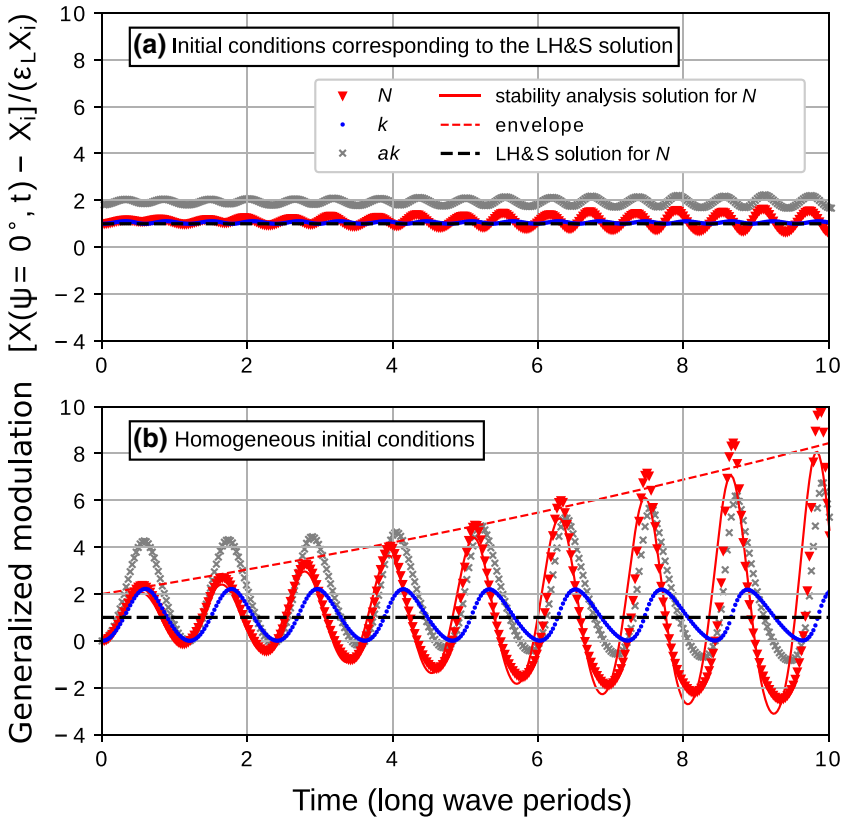

Figure 2. Time evolution of the relative change of the modulation of wave action N, wave number k and steepness ak following long wave crests for a short waves train with $k_i/k_L = 10$, $\varepsilon_L = 0.1$, $\gamma_i = 1$ and Co = 0.1. Panel (a) corresponds to LH&S initial conditions $M_{N,i} = M_{k,i} = 1$, and panel (b) to homogeneous initial conditions $M_{N,i} = M_{k,i} = 0$ as in Figure 1. The stability analysis solution and its envelope correspond to the analytical solution of Appendix C.

keeps growing at each cycle. This leads to a pattern of very sharp action maxima that travels along the long wave profile at a speed that is, very close to the short wave group speed (dotted lines in Figure 1). Every time the maximum goes over the crest of a long wave it is amplified a little more.

A more quantitative understanding is provided by the time evolution of both the wave action and the wave number modulations as presented in Figure 2 following a long wave crest, that is, $\psi = 0^\circ$, corresponding to a vertical slice through Figure 1. Two simulations are shown starting from either the modulated LH&S profile ($M_{N,i} = M_{k,i} = 1$) or a uniform distribution along the long wave profile ($M_{k,i} = M_{N,i} = 0$). This second option corresponds to the sudden appearance of a long wave perturbation in the middle of a homogeneous short wave field. It is less clear under which the first option may be realized, given that the solution appears to be unstable. Indeed, the top panel suggests that the LH&S solution is much more stable with modulations locked in phase with the long wave crests and an amplitude of 1, but still the numerical solution slowly deviates and produces higher and lower values of N and k.

In general, the modulation of k is less pronounced than the modulation of N. The time evolution of k is given by Equation 15 alone, as C is a function of k only, and develops into the typical saw-tooth profile due to the nonlinearity brought by the piece of the advection velocity (the short wave phase speed) that is, proportional to $k^{-0.5}$. This is similar to the formation of shocks for shoaling waves in the shallow water equation. Such a formation of shocks is a common property of all nonlinear Burgers-type advection equations (Whitham, 1974). The numerical scheme here does not fully capture the shocks and keeps them relatively smooth.

The combined behavior of N and k leads to a progressive steepening of the short waves, due to the growth of the wave action peaks almost in phase with those of the wave number (see Figure 2). Again, while

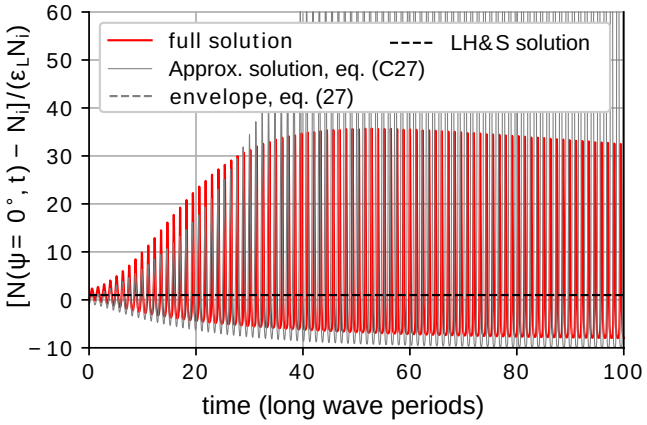

Figure 3. Wave action modulation on wave crests (same case as Figure 2b for a longer time range).

the steepness of the LH&S initial conditions almost does not evolve, the maximum steepness from any other cosine-distributed initial condition is much larger.

The longer term evolution shown in Figure 2 later has M_N exceeding 10 after 10 long wave periods. This focusing is typical of Burgers-type advection equations. The later stabilization at $M_N \approx 40$ for larger times (see Figure 3) is beyond the scope of the present paper and may be due to numerical diffusion. Anyway, such large values should never be reached for short waves with average steepness $ak > 0.1$ in the presence of long waves with similar steepness, because short wave breaking should occur before.

The growth of the wave action disappears when the advection is linearized, as done by LH&S, when neglecting the $\partial_x C_g$ terms in both Equations 2 and 3 compared to $\partial_x U$.

3.2. Stability Analysis

The behavior of the short waves is investigated analytically in a weak nonlinear interactions framework by switching to the alternative set of Equations 16 and 17, with initial conditions 22 and 24. The procedure used to solve this problem is detailed in Appendix C for the 2D and summarized here in the 1D case. Using a classical perturbation expansion in powers of the long wave steepness ε_L, the perturbation induced by the long waves modulation through the first order solution $\{N_1, C_1\}$ on the initial state $\{N_0, C_0\}$ follows (see Appendix C)

$$\left[\partial_t + \left(C_0 / 2\right)\partial_x\right]N_1 = -N_0\partial_x U - \left(N_0 / 2\right)\partial_x C_1 \tag{25}$$

$$\left[\partial_t + \left(C_0 / 2\right)\partial_x\right]C_1 = \left(C_0 / 2\right)\partial_x U + C_0 / \left(2g\right)\left(\partial_t + C_0\partial_x\right)g'. \tag{26}$$

Already the sources of the instability are visible. There is a single way coupling occurring here. The evolution of C_1 given by Equation 26 is stand-alone, and is plugged into the one of N_1 through the right-hand side of Equation 25. As both equations have the same left-hand side operator, they have the same natural frequency. The forcing operated by the term $\partial_x C_1$ in the Equation 25 forces N_1 at its resonance frequency (secular term), giving rise to an exponential growth of the solution. That term was precisely neglected by LH&S.

In that case, the perturbative expansion cannot be applied, and approximate solutions are obtained using a multiple time scale method (see Appendix C). Especially, the resonance results in an exponential growth of the wave action maxima (the total wave action being conserved) with typical e-folding time τ estimated from (93), which reduces to

$$\frac{1}{\tau} = \left|\Omega\right| \simeq \frac{1}{4}\varepsilon_L\sigma_L\frac{C_i}{C_L}\left|1 - M_{k,i}\right| \tag{27}$$

assuming a 1D case and using $C_i/C_L \ll 1$. This expression is valid for times $\mathcal{O}\left(\varepsilon_L^{-1}\right)$, typically of the order 10 long wave periods. The growth which takes place does not change the total wave action over the long wave profile, but modifies its distribution as explained in the previous section. A comparison of the approximate solution with the numerical simulation of the previous paragraph is presented in Figure 3 (gray lines). For most cases, the growth predicted theoretically is first slower than the one modeled, overpasses it at large enough times, but still presents a behavior to the one computed numerically.

The influence of initial conditions on the growth of the solution is presented in Figure 4. For both the numerical and the stability analysis solution, this diagram clearly highlights an unstable equilibrium position around the LH&S initial conditions. More precisely, for the analytical solution, a stationary solution is obtained when

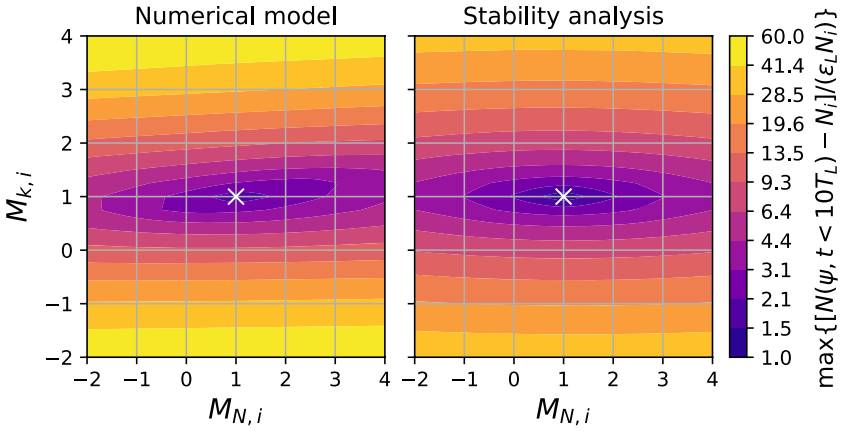

Figure 4. Maximum action modulation after 10 long wave periods from initiation as a function of various initial modulations. The runs are performed with $k_i/k_L = 10$, $\varepsilon_L = 0.1$, $\gamma_i = 1$ and Co = 1. The white crosses stand for LH&S initial conditions $M_{N,i} = M_{k,i} = 1$.

$$M_{k,i} = M_g - 2\frac{\mu}{\chi} \simeq 1, \tag{28}$$

and the oscillations of the action profile are cancelled when

$$M_{N,i} = \frac{\mu'}{\chi} \simeq 1, \tag{29}$$

where μ, χ and μ' are defined in Appendix C, Equations C24, C25, and C29. The combination of Equations 28 and 29 is very close to the LH&S solution. The exact stationary profile in 1D was studied by Kharif (1990) and deviates slightly from a linearly modulated profile such as the ones taken as initial conditions. From Figure 4, the furthest the initial conditions from the stationary solution, the larger the oscillations of the solution around the stationary profile, and the largest the growth of action. It has to be noted that the modulation on k has more significant consequences on the growth of action than the modulation of action itself.

4. Modulation of Noncollinear Wave Trains

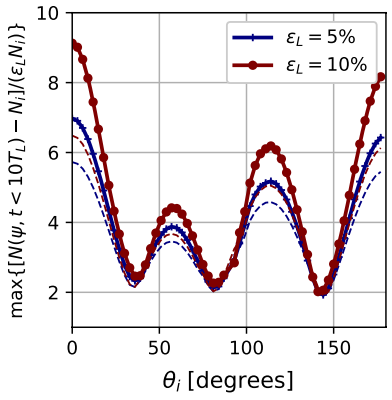

Figure 5. Angular profile of action modulation maxima at the long waves crests over 10 long wave periods from initiation in the case $M_{N,i} = M_{k,i} = 0$, $\varepsilon_L = 0.1$, $k_i/k_L = 10$, $\gamma_i = 1$ and Co < 0.1. The dashed lines are given by our analytical model.

Numerical simulations and analytical calculations, detailed in Appendix C, have been performed for short waves propagating at an angle relative to the long wave propagation, that is, with $\gamma < 1$. Both results are illustrated in Figure 5. The calculations predict a growth of the wave action at the rate

$$\frac{1}{\tau} = |\Omega| \simeq \frac{1}{4}\varepsilon_L \sigma_L \frac{C_i}{C_L}\left|\gamma_i\left(1 - M_{k,i}\right)\left(3\gamma_i^2 - 2\right)\right|, \tag{30}$$

as given by Equation C27, with $C_i / C_L \ll 1$.

The maxima of wave action modulation after 10 long wave periods are presented for two different long wave steepnesses $\varepsilon_L = 0.05$ and $\varepsilon_L = 0.1$ (solid lines), and compared to the predictions of our analytical model, Equation 66 (dashed lines). The same qualitative behaviors are observed for both the analytical and the numerical solutions. The largest errors of the analytical model are found where the growth rate is the largest. Indeed, the exponential growth expected in the stability analysis generally

underestimates the growth of the numerical solution at early times. However, the general directional distribution is well captured. Especially, the growth rate Equation (30) becomes zero at $\gamma_i = \pm\sqrt{2/3}$ which corresponds to $\theta_i \simeq 35^\circ$ and $\theta_i \simeq 145^\circ$. These angles define a ±35° sector around the upwave and downwave directions for which an excess breaking probability of short waves can be expected.

Qualitatively, the behavior of the noncollinear solutions is similar to collinear wave trains. There still exists for each initial direction θ_i a stationary solution, for which modulation does not change, given at order ε_L by expressions (28) and (29). For given cosine-distributed initial conditions, the distance of the initial modulation from the stationary solution determines both the amplitude of the subsequent modulation and instability.

5. Discussion and Conclusions

From our analysis we found that short waves modulation by monochromatic long waves can be more complex than the steady cosine shape variation in wave action and wavenumber given by the linearized solution of Longuet-Higgins and Stewart (1960). For a wide class of initial conditions, the short wave energy condenses into very steep and narrow wave packets around the long wave crests. This resonance mechanism is expected to occur for other kinds of dispersive wave interactions, in particular for gravity waves in intermediate water depth. It can also be expected for any kind of dispersive wave packet periodically forced in space and time by an external source. A similar mechanism has already been reported and measured experimentally for the interaction between a surface and an internal gravity waves by Lewis et al. (1974), with a maximum of the interaction when the phase speed of the long wave matches the group speed of the short waves, corresponding to $\chi = 0$ in the analysis reported in Appendix C.

Although the qualitative behavior is the same regardless of the initial conditions, both the oscillations and the growth rate Equation 27 depend on the initial conditions, especially on the magnitude of the short wave perturbation along the long wave profile. There exists a stationary profile of short waves, close to the LH&S solution, but any deviation from that profile results in an exponential growth of the wave action maxima. Ultimately, this should lead to a steepening of the short waves profile and an increase of the breaking probability.

For a wide range of initial conditions there is locally, after about 10 long waves periods, an effect of the long waves on the short waves that is, 10 times larger than expected by LH&S. This effect is maximum for short and long wave propagating in the same direction, and is greatly reduced for direction differences larger than 20 degrees. Over this time scale, considering the empirical growth term of Plant (1982), the wind-wave generation can only be neglected for winds under 3 m/s or short wavelengths longer than 1 m. In these conditions, the occurrence of extreme short wave amplitude may be governed by the process described here. In order to be applied to the analysis of meter-scale wave breaking in the presence of longer waves, the instability of short wave packets that we describe here should be investigated in a more realistic setting. In particular, we expect that replacing the monochromatic long waves by random long wave groups will limit the magnitude of the maximum steepness as the forcing will only be coherent over only 10 or so long wavelengths. Also, this model may not be valid for all waves in a broad wind wave spectrum, as a scale separation assumption is required. Finally, the present theoretical framework is limited to order ε_L^1 solutions, and cannot be applied at long time scales for which nonlinear 4-wave resonant interactions will likely dominate the evolution of the wave field (Hasselmann, 1962).

In the ocean, short gravity waves ride on a random superposition of waves that is, different from the monochromatic waves investigated here. We expect that significant modulations can be generated over the time scale of a few long wave periods, with oscillations around the LH&S solution. Future analysis may further combine generation and dissipation effects with the conservative case described here, possibly following Longuet-Higgins (1991). The short wave response to wave groups is another topic that should be investigated as a step toward a practical application for the parameterizations of spectral wave evolution.

Appendix A: Alternative Set of Equations

Equation for the phase speed C

Equation 15 is rewritten as a function of $C = \sqrt{g' / k}$. From the chain rule, the derivatives of C and k_x are connected through

$$dC = \frac{\partial C}{\partial k_x} dk_x + \frac{\partial C}{\partial g'} dg'. \tag{A1}$$

Knowing that $\partial C / \partial k_x = -\gamma C / \left(2k\right)$ and $\partial C / \partial g' = C / \left(2g'\right)$, then

$$\begin{aligned} \partial_t C &= -\gamma C / \left(2k\right)\partial_t k_x + C / \left(2g'\right)\partial_t g' \\ &= \gamma C / \left(2k\right)\partial_x \left[\left(C / \left(2\gamma\right) + U\right)k_x\right] + C / \left(2g'\right)\partial_t g' \end{aligned} \tag{A2}$$

from Equation 15. The x derivatives are then expanded and expressed as a function derivatives of C only. Especially, from Appendix A1,

$$\partial_x k_x = -\frac{2k}{\gamma C}\partial_x C + \frac{k}{\gamma g}\partial_x g', \tag{A3}$$

and

$$\partial_x \gamma = \partial_x \left(k_x / k\right) = \frac{1-\gamma^2}{k}\partial_x k_x = \frac{\gamma^2 - 1}{2\gamma C}\left[\partial_x C - C / \left(2g'\right)\partial_x g'\right], \tag{A4}$$

as $dk_x = \gamma dk$. After collecting the $\partial_x C$ terms in Appendix A2 using Appendices A3 and A4, Equation 17 is obtained.

The initial condition on C can be derived from the one on k_x, Equation 23:

$$C\left(t = 0\right) = \sqrt{g' / k\left(t = 0\right)} \tag{A5}$$

$$= \sqrt{g\left(1 + \varepsilon_L M_g \cos\psi\right) / \sqrt{k_i^2 \gamma_i^2 \left(1 + \varepsilon_L M_{k,i} \cos\psi\right)^2 + \left(1 - \gamma_i^2\right)k_i^2}} \tag{A6}$$

$$= C_i\left(1 + \varepsilon_L M_{C,i} \cos\psi\right) + \mathcal{O}\left(\varepsilon_L^2\right), \tag{A7}$$

where

$$C_i = \sqrt{\frac{g}{k_i}} \tag{A8}$$

and

$$M_{C,i} = \frac{M_g - \gamma_i^2 M_{k,i}}{2}. \tag{A9}$$

A.2. Equation for N

Although Equation 14 is already expressed as a function of N and C, it can be expressed in a more convenient way by expanding the x-derivative term. Especially:

$$\begin{aligned}\partial_t N + \frac{\gamma}{2} C \partial_x N &= -N\partial_x\left(\frac{\gamma}{2}C\right) - N\partial_x U \\ &= -\left(N\gamma\,/\,2\right)\partial_x C - \left(NC\,/\,2\right)\partial_x\gamma - N\partial_x U.\end{aligned} \tag{A10}$$

Then, using Equation A4 and collecting terms in $\partial_x C$, Equation 16 is obtained.

Appendix B: Numerical Scheme

General Procedure

Any of the above equations can be translated in the frame moving with the long wave phase speed through a change of coordinates from (x,t) to (ψ,T) where ψ is the long wave phase and $T = \sigma_L t$ accompanied with a change of variables from N and k_x to $q = (\alpha,\kappa_x)$, where

$$\alpha = N(\psi,T)\,/\,N_i \tag{B1}$$

$$\kappa_x = \gamma\kappa = k_x(\psi,T)\,/\,k_L. \tag{B2}$$

Equations 14 and 15 are then written in a nonlinear advection form

$$\partial_T \boldsymbol{q} + \partial_\psi f(\boldsymbol{q},\psi) = 0. \tag{B3}$$

The flux function f is split into a quasi-linear term g and a ψ-dependent source term s

$$f(\boldsymbol{q},\psi) = g(\boldsymbol{q}) + s(\boldsymbol{q},\psi) \tag{B4}$$

with

$$g(\boldsymbol{q}) = \left[\left(\frac{\gamma}{2}\kappa^{-0.5} - 1\right)\alpha, \left(\frac{\kappa^{-0.5}}{\gamma} - 1\right)\kappa_x\right] \tag{B5}$$

and

$$s(\boldsymbol{q},\psi) = \varepsilon_L \cos\psi\boldsymbol{q} + \kappa^{-0.5}\left(\sqrt{1+\varepsilon_L\cos\psi} - 1\right)\left[\left(\gamma\,/\,2\right)\alpha,\kappa_x\,/\,\gamma\right], \tag{B6}$$

which includes the contributions of the orbital currents and the apparent gravity. Here, both functions are nonlinear, which requires a careful choice of numerical methods. We verified numerically that the scheme is conservative, in the sense that both the total action and wave number over the whole numerical domain (a long wave phase) are conserved during the time integration, within the round-off error.

The combination of a Runge-Kutta order 4 and the MUSCL4 numerical scheme of Kurganov and Tadmor (2000) is found to provide satisfying results for the numerical solution of the advection-only system and for the stability of the full solution computation. The Runge-Kutta scheme is used to solve the ODE

$$Q_j'(\tau) = -\frac{1}{\Delta x}\left(F^n_{j+1/2} - F^n_{j-1/2}\right), \tag{B7}$$

where discretized quantities are indexed with j and $F^n_{j\pm1/2}$ corresponds to MUSCL numerical fluxes. The latter are computed according to

$$F^n_{j+1/2} = \frac{1}{2}\left[g\left(Q^R_{j+1/2}\right) + g\left(Q^L_{j+1/2}\right)\right) - \lambda^{\max}\left(Q^R_{j+1/2} - Q^L_{j+1/2}\right) \left(+s\left(Q^n_{j+1}\right) - s\left(Q^n_{j-1}\right)\right] \quad \text{(B8)}$$

where

$$\boldsymbol{Q}^R_{j+1/2} = \boldsymbol{Q}^n_{j+1} - \frac{\Delta x}{2}\boldsymbol{\sigma}^n_{j+1} \quad \text{(B9)}$$

$$\boldsymbol{Q}^L_{j+1/2} = \boldsymbol{Q}^n_{j} + \frac{\Delta x}{2}\boldsymbol{\sigma}^n_{j} \quad \text{(B10)}$$

$$\boldsymbol{\sigma}^n_j = \text{minmod}\left(\frac{\boldsymbol{Q}^n_j - \boldsymbol{Q}^n_{j-1}}{\Delta x}, \frac{\boldsymbol{Q}^n_{j+1} - \boldsymbol{Q}^n_j}{\Delta x}\right) \quad \text{(B11)}$$

where minmod (a, b) is equal to

$$0 \text{ if } ab < 0 \text{ B12} \quad \text{(B12)}$$

$$a \text{ if } ab > 0, \quad \text{and} \quad |a| < |b| \quad \text{(B13)}$$

$$b \quad \text{if} \quad ab > 0, \quad \text{and} \quad |a| > |b| \quad \text{(B14)}$$

$$\lambda^{\max} = \max\left(\lambda^R, \lambda^L\right) \quad \text{(B15)}$$

$$\lambda^R = \left[\max_j \left|-1 + \gamma_j \,/\, 2\left(\kappa^R_j\right)^{-0.5}\right|, \max_j \left|-1 + 1 \,/\, \left(2\gamma_j\right)\left(\kappa^R_j\right)^{-0.5}\right|\right] \quad \text{(B16)}$$

are the maximum wave speeds at a given time step (eigenvalues of the Jacobian matrix g') and where κ^R_j is computed according to Equation B9.

The numerical resolution uses 128 points over the long wave wavelength, with periodic boundary conditions $q\left(\psi = 360^\circ, T\right) = q\left(\psi = 0^\circ, T\right)$. The time step is chosen so that the Courant number Co is lower or equal to one

$$\Delta T = \frac{Co\Delta\psi}{\lambda^{\max}}, \quad \text{(B17)}$$

thus insuring the stability of the numerical scheme. As $\lambda^{\max} \simeq 1$, the typical time step is $\Delta T \simeq 1 \,/\, 128$ long wave periods.

B.2. Test Case

The numerical scheme was tested against the closest analytically solvable problem

$$\partial_t X + \partial_x\left[U\left(x,t\right)X\right] = 0. \quad \text{(B18)}$$

verified both by $X = N$ and $X = k_x$, which are the same as Equations 14 and 15 without the self-advection term and the apparent gravity modification, or equivalent to reducing f in Equation B4 to

$$f\left(\boldsymbol{q},\psi\right) = \left(-1 + \varepsilon_L \cos\psi\right)\boldsymbol{q}. \tag{B19}$$

With initial condition $X\left(x,t=0\right) = X_i\left(1 + \varepsilon_L M_{X,i}\cos\psi\right)$ and in the case of a monochromatic long wave orbital current Equation 8, the solution of Equation B18 is:

$$X\left(x,t\right) = X_i \frac{v\left[\sigma_L t + u\left(\psi\right)\right]}{1 - \varepsilon_L \cos\psi}, \tag{B20}$$

where

$$u\left(\psi\right) = 2 \,/\, \sqrt{1-\varepsilon_L^2}\,\arctan\left[\sqrt{\left(1+\varepsilon_L\right)/\left(1-\varepsilon_L\right)}\tan\left(\psi \,/\, 2\right)\right] \tag{B21}$$

$$v\left(\psi\right) = 1 + \varepsilon_L\left(M_{X,i} - 1\right)r\left(\psi\right) - \varepsilon_L^2 M_{X,i} r^2\left(\psi\right) \tag{B22}$$

$$r\left(\psi\right) = \left[1 - w^2\left(\psi\right)\right] / \left[1 + w^2\left(\psi\right)\right] \tag{B23}$$

$$w\left(\psi\right) = \sqrt{\left(1-\varepsilon_L\right)/\left(1+\varepsilon_L\right)}\tan\left(\sqrt{1-\varepsilon_L^2}\psi \,/\, 2\right). \tag{B24}$$

The classical Lax-Wendroff scheme for nonlinear advection equations (Leveque, 2002) has been tested but unrealistically overestimates the growth of instability, contrary to the present scheme. As a drawback, when compared to the analytical solution (B20), the present scheme exhibits a slightly lower accuracy than the Lax-Wendroff scheme. Although conservative, the distributions of N and k_x flatten spatially due to MUSCL-RK4. The mean error typically increases by 3% every 100 long waves periods for Co = 1 and 128 spatial samples.

Appendix C: Multiple Time Scales Modulated Fields at Order ε_L

Here, we look for spatially periodic solutions for the short waves field by switching from the set of Equations 14 and 15 on N and k_x to the alternative set Equations 14 and 17 on N and C, the equation on C being more convenient algebraically than the one on k_x. Initial conditions (22) and (24) must be associated with the present set of equations. The variables are then expanded in powers of the small parameter ε_L:

$$N = N_0 + \varepsilon_L N_1 + \mathcal{O}\left(\varepsilon_L^2\right) \tag{C1}$$

$$C = C_0 + \varepsilon_L C_1 + \mathcal{O}\left(\varepsilon_L^2\right). \tag{C2}$$

Similarly, for γ, which is a function of C only, we have:

$$\gamma = \gamma_0 + \varepsilon_L \gamma_1 + \mathcal{O}\left(\varepsilon_L^2\right). \tag{C3}$$

At order ε_L^0, Equations 16 and 17 and their initial conditions are

$$\left(\partial_t + \gamma_0 C_0 \,/\, 2\partial_x\right)N_0 = -N_0\left(3\gamma_0^2 - 2\right) / \left(2\gamma_0\right)\partial_x C_0 \tag{C4}$$

$$\left(\partial_t + \gamma_0 C_0 \,/\, 2\partial_x\right)C_0 = 0 \tag{C5}$$

$$N_0\left(t=0\right) = N_i \tag{C6}$$

$$C_0\left(t=0\right) = C_i. \tag{C7}$$

which are nonlinear forced advection equations. For simplicity, we consider the ε_L^0 solutions to be constant throughout the propagation, although this system of equations would allow for more complicated solutions. Hence we consider:

$$N_0\left(x,t\right) = N_i \tag{C8}$$

$$C_0\left(x,t\right) = C_i, \tag{C9}$$

and consequently

$$\gamma_0\left(x,t\right) = \gamma_i \tag{C10}$$

At order ε_L, the equations to be solved are

$$\begin{aligned}\left[\partial_t + \left(\gamma_0 C_0 \,/\, 2\right)\partial_x\right]N_1 &= -N_0 \,/\, \varepsilon_L \partial_x U - N_0\left(3\gamma_0^2 - 2\right) / \left(2\gamma_0\right)\partial_x C_1 \\ &-N_0 C_0\left(1-\gamma_0^2\right) / \left(2\varepsilon_L g \gamma_0\right)\partial_x g'\end{aligned} \tag{C11}$$

$$\left[\partial_t + \left(\gamma_0 C_0 \,/\, 2\right)\partial_x\right]C_1 = \left(\gamma_0^2 C_0 \,/\, 2\right)\partial_x U + C_0 \,/\, \left(2\varepsilon_L g\right)\left(\partial_t + \gamma_0 C_0 \partial_x\right)g' \tag{C12}$$

$$N_1\left(t=0\right) = N_i M_{N,i}\cos\psi \tag{C13}$$

$$C_1\left(t=0\right) = C_i M_{C,i},\cos\psi \tag{C14}$$

because U is a ε_L order function, according to Equation 8.

In the present case, the solution of the system Equations C11–C14 would invalidate the perturbative expansion performed so far. Indeed, as it is discussed in Section 33.2, this system presents a secular term $-N_0\left(3\gamma_0^2 - 2\right) / \left(2\gamma_0\right)\partial_x C_1$ in Equation C11. Its analytical solution would result in an unbounded growth of the solution N_1 namely, or instability. As a consequence, at large enough times, N_1 would become greater than N_0, which would be in contradiction with the assumptions behind the perturbative expansion Equation C1. This was not considered in LH&S.

As an alternative to the perturbative expansion performed until now, and in the presence of a secular term, a multiple scale method can be employed (e.g., Nayfeh, 1973) to revisit the problem from the beginning. This methods consists in keeping the perturbative expansion Equations C1 and C2, and completing it by replacing the single time dimension by two. Two time scales are introduced, a fast one, $t_0 = t$ and a slow one, $t_1 = \varepsilon_L t$. t_0 is the scale of the regular oscillations, while t_1 is the scale of the instability. In the multiple scale method, these two variables are considered as independent. This introduces a single modification in the previous derivations. The time derivative is changed into

$$\partial_t = \partial_{t_0} + \varepsilon_L \partial_{t_1} \tag{C15}$$

At order ε_L^0, Equations C4–C7 remain true only by replacing t by t_0. The solutions Equations C8 and C9 are kept, but the dependency on t_1 is not solved. In other words

$$N_0\left(t_0,t_1,x\right) = N_i + N_0^{'}\left(t_1\right) \tag{C16}$$

$$C_0\left(t_0,t_1,x\right) = C_i + C_0^{'}\left(t_1\right). \tag{C17}$$

At order ε_L^1, changes appear due to the introduction of the instability time. t_1 derivatives of N_0 and C_0, respectively, are added in Equations C11 and C12, according to Equation C15. In the multiple time scales

method, the slow time derivative terms are here to balance the secular terms, so that we are left with, on the one side,

$$\left[\partial_{t_0} + \left(\gamma_0 C_0 / 2\right)\partial_x\right] N_1 = -\left(N_0 / \varepsilon_L\right)\partial_x U - N_0 C_0\left(1 - \gamma_0^2\right) / \left(2g\varepsilon_L\gamma_0\right)\partial_x g' \tag{C18}$$

$$\left[\partial_{t_0} + \left(\gamma_0 C_0 / 2\right)\partial_x\right] C_1 = \gamma_0^2 C_0 / \left(2\varepsilon_L\right)\partial_x U + C_0 / \left(2\varepsilon_L g\right)\left(\partial_{t_0} + \gamma_0 C_0 \partial_x\right) g', \tag{C19}$$

and on the other,

$$d_{t_1} N_0{}' = -N_0\left(3\gamma_0^2 - 2\right) / \left(2\gamma_0\right)\partial_x C_1 \tag{C20}$$

$$d_{t_1} C_0{}' = 0. \tag{C21}$$

with still the same initial conditions Equations C13 and C14. The solutions are obtained by solving for Equations C18 and C19 alone first, and introducing their solutions into the instability Equations C21 and C22.

The full solutions are summarized here. The phase speed consists in an average constant value

$$C_0 = C_i = \sqrt{\frac{g}{k_i}} \tag{C22}$$

modulated with a fixed amplitude

$$C_1 = C_i\left[\left(M_{C,i} - \frac{\mu}{\chi}\right)\cos\left(\psi + \sigma_L\chi t\right) + \frac{\mu}{\chi}\cos\psi\right] \tag{C23}$$

where the constants χ and μ are defined by

$$\chi = 1 - 0.5\gamma_i C_i / C_L \tag{C24}$$

$$\mu = -\gamma_i^2 / 2 + M_g / 2\left(1 - \gamma_i C_i / C_L\right) \tag{C25}$$

and where the initial modulation on C is given by Equation A9. The action is already distorted at order ε_L^0:

$$N_0 = N_i \exp\left[\Omega t \sin\left(\psi + \sigma_L\chi t\right)\right] \tag{C26}$$

where

$$\Omega = \frac{1}{4}\varepsilon_L\sigma_L\frac{C_i}{\chi C_L}\left[\gamma_i\left(1 - \chi M_{k,i}\right) + \frac{M_g}{2}\frac{C_i}{C_L}\right]\left(3\gamma_i^2 - 2\right). \tag{C27}$$

with an additional modulation at order ε_L^1:

$$N_1 = N_i\left[\left(M_{N,i} - \frac{N_0}{N_i}\frac{\mu'}{\chi}\right)\cos\left(\psi + \sigma_L\chi t\right) + \frac{N_0}{N_i}\frac{\mu'}{\chi}\cos\psi\right], \tag{C28}$$

where

$$\mu' = 1 - \frac{1}{4}\frac{C_i}{\chi C_L}\left\{\gamma_i\left(3\gamma_i^2 - 2\right) - M_g\left[\gamma_i - \frac{C_i}{C_L}\left(2\gamma_i^2 - 1\right)\right]\right\} \tag{C29}$$

The 1D solutions of Section 3 are obtained by setting $\gamma_i = 1$.

Acknowledgments
This study is a purely theoretical work and does not use any data. Charles Peureux, Fabrice Ardhuin, and Pedro Veras Guimarães were supported by CNES as part of the SKIM preparation program and ANR grants for ISblue (ANR-17-EURE-0015) LabexMER (ANR-10-LABX-19), and MIMOSA (ANR-14-CE01-0012).

References

Ardhuin, F., Dumas, F., Bennis, A.-C., Roland, A., Sentchev, A., Forget, P., et al. (2012). Numerical wave modeling in conditions with strong currents: Dissipation, refraction and relative wind. *Journal of Physical Oceanography*, *42*, 2101–2120.

Ardhuin, F., Rogers, E., Babanin, A., Filipot, J.-F., Magne, R., Roland, A., et al (2010). Semi-empirical dissipation source functions for wind-wave models: Part I, definition, calibration and validation. *Journal of Physical Oceanography*, *40*(9), 1917–1941. https://doi.org/10.1175/2010JP04324.1

Banner, M. L., Gemmrich, J. R., & Farmer, D. M. (2002). Multiscale measurement of ocean wave breaking probability. *Journal of Physical Oceanography*, *32*, 3364–3374. Retrieved from http://ams.allenpress.com/archive/1520-0485/32/12/pdf/i1520-0485-32-12-3364.pdf

Banner, M. L., Jones, I. S. F., & Trinder, J. C. (1989). Wavenumber spectra of short gravity waves. *Journal of Fluid Mechanics*, *198*, 321–344.

Banner, M. L., & Morison, R. P. (2010). Refined source terms in wind wave models with explicit wave breaking prediction. part I: Model framework and validation against field data. *Ocean Modelling*, *33*, 177–189. https://doi.org/10.1016/j.ocemod.2010.01.002

Bretherton, F. P., & Garrett, C. J. R. (1968). *Wavetrains in inhomogeneous moving media* (Vol. A302, pp. 529–554). Proceedings of the Royal Society of London.

Donelan, M. A., Curcic, M., Chen, S. S., & Magnusson, A. K. (2012). Modeling waves and wind stress. *Journal of Geophysical Research*, *117*, C00J23. https://doi.org/10.1029/2011JC007787

Elfouhaily, T., Thompson, D. R., Chapron, B., & Vandemark, D. (2001). Improved electromagnetic bias theory: Inclusion of hydrodynamic modulations. *Journal of Geophysical Research*, *106*(C3), 4655–4664.

Garrett, C., & Smith, J. (1976). On the interaction between long and short surface waves. *Journal of Physical Oceanography*, *6*, 925–930.

Hara, T., Hanson, K. A., Bock, E. J., & Uz, B. M. (2003). Observation of hydro-dynamic modulation of gravity-capillary waves by dominant gravity waves. *Journal of Geophysical Research*, *108*(C2), 3028. https://doi.org/10.1029/2001JC001100

Hasselmann, K. (1962). On the non-linear energy transfer in a gravity wave spectrum, part 1: General theory. *Journal of Fluid Mechanics*, *12*, 481–501.

Hasselmann, K. (1971). On the mass and momentum transfer between short gravity waves and larger-scale motions. *Journal of Fluid Mechanics*, *4*, 189–205.

Hasselmann, K., Raney, R. K., Plant, W. J., Alpers, W., Shuchman, R. A., Lyzenga, D. R., et al. (1985). Theory of synthetic aperture radar ocean imaging: A MARSEN view. *Journal of Geophysical Research*, *90*(C3), 4659–4686.

Keller, W. C., & Wright, J. W. (1975). Microwave scattering and the straining of wind-generated waves. *Radio Science*, *10*, 139–147.

Kharif, C. (1990). Some aspects of the kinematics of short waves over longer gravity waves on deep water. In A. Tørum, & O. T. Gudmestad (Eds.), *Water wave kinematics* (pp. 265–279). Springer Netherlands.

Kurganov, A., & Tadmor, E. (2000). New high-resolution central schemes for nonlinear conservation laws and convection-diffusion equations. *Journal of Computational Physics*, *160*, 241–282.

Leckler, F., Ardhuin, F., Peureux, C., Benetazzo, A., Bergamasco, F., & Dulov, V. (2015). Analysis and interpretation of frequency-wavenumber spectra of young wind waves. *Journal of Physical Oceanography*, *45*, 2484–2496. https://doi.org/10.1175/JP0-D-14-0237.1

Leveque, R. J. (2002). *Finite volume methods for hyperbolic problems*. Cambridge, UK: Cambridge University Press.

Lewis, J. E., Lake, B. M., & Ko, D. R. S. (1974). On the interaction of internal waves and surface gravity waves. *Journal of Fluid Mechanics*, *63*, 773–800.

Longuet-Higgins, M. S. (1969). Action of a variable stress at the surface of water waves. *Physics of Fluids*, *12*(4), 737–740.

Longuet-Higgins, M. S. (1991). A stochastic model of sea-surface roughness. II. *Proceedings of the Royal Society of London*, *435*, 405–422.

Longuet-Higgins, M. S., & Stewart, R. W. (1960). Changes in the form of short gravity waves on long waves and tidal currents. *Journal of Fluid Mechanics*, *8*, 565–583.

Munk, W. H., Miller, G. R., Snodgrass, F. E., & Barber, N. F. (1963). Directional recording of swell from distant storms. *Philosophical Transactions of the Royal Society of London - A*, *255*, 505–584.

Nayfeh, A. H. (1973). *Perturbation methods*, Wiley-Interscience.

Peureux, C. (2017). *Observation et modelisation des proprietes directionnelles des ondes de gravite courtes (Unpublished doctoral dissertation)*. Brest, France: Université de Bretagne Occidentale, Ecole doctorale des Sciences de la Mer et du Littoral.

Peureux, C., Benetazzo, A., & Ardhuin, F. (2018). Note on the directional properties of meter-scale gravity waves. *Ocean Science*, *14*, 41–52. https://doi.org/10.5194/os-14-41-2018

Phillips, O. M. (1977). *The dynamics of the upper ocean* (p. 336). London: Cambridge University Press.

Phillips, O. M. (1985). Spectral and statistical properties of the equilibrium range in wind-generated gravity waves. *Journal of Fluid Mechanics*, *156*, 505–531.

Plant, W. J. (1982). A relationship between wind stress and wave slope. *Journal of Geophysical Research*, *87*, 1961–1967.

Romero, L. (2019). Distribution of surface wave breaking fronts. *Geophysical Research Letters*, *46*, 10463–10474. https://doi.org/10.1029/2019GL083408

Whitham, G. B. (1974). *Linear and nonlinear waves* (p. 636). New York: Wiley.

Zhang, J., & Melville, W. K. (1981). On the stability of weakly nonlinear short waves on finite-amplitude long gravity waves. *Journal of Fluid Mechanics*, *242*, 51–72.